Quantum Limits to the Force Sensitivity of a Micromechanical Resonator Observed by an Optical Interferometer and Implications for the Large-Scale Simulation of Quantum Systems

Lee E. Harrell
Department of Physics
U. S. Military Academy, West Point, New York

Sponsor: John A. Sidles
Department of Orthopædics and Sports Medicine
University of Washington, Seattle, WA

1 Executive Summary

Optical interferometers are commonly used to observe the oscillations of micromechanical force sensors with great precision. Picometer-scale oscillations—a factor of 10^6 smaller than the wavelength of the light used to observe them—are readily observable with fiber optic interferometers constructed from off-the-shelf components [1], and thermally driven Brownian motion is observable in well-isolated micromechanical oscillators at millikelvin temperatures [2].

While state-of-the-art force measurements are limited by thermal fluctuations of the oscillator, the drive towards atomic-resolution imaging of protons by magnetic resonance force microscopy (MRFM) [3] raises the question of the ultimate limits of interferometer sensitivity. In these experiments, both the interferometer light and the mechanical oscillator have the potential to exhibit quantum behavior, and a microscopic model of their interaction is necessary for a full analysis. We present a microscopic model of this interaction based on entanglement of interferometer photons with the mechanical oscillator and analyze the photon back-action on the oscillator. The quantum analysis predicts a minimum noise power spectral density in the force data of

$$S_{F\,\text{measured}} = \sqrt{2}k_s\hbar\,, \tag{1.1}$$

where $\hbar$ is Planck's constant and k_s is the spring constant of the mechanical oscillator.

The same measurement formalism is a central element of a broader research program whose strategic objective is the efficient simulation of large-scale quantum systems. Examples of such systems include biological molecules and spintronic devices [4]. These quantum systems are typically coupled to both to readout devices (e.g., nanoscale cantilevers and field-effect transistors) and to ambient thermal fluctuations. At present, the best-known algorithms for simulating such systems require exponentially large computing resources as the number of degrees of freedom of the system increases. We discuss a new class of simulation algorithms in

which the ambient thermal fluctuations are modeled as additional, simultaneous measurement processes. When this substitution is made, the computing resources required to accurately simulate the system increase as a polynomial function of the number of degrees of freedom. These new algorithms, if they fulfill their early promise, will allow the engineering design of complex quantum technologies to proceed with confidence that "if we build it, it will work."

2 Introduction

2.1 Magnetic Resonance Force Microscopy

MRFM, a scanned-probe force microscopy first proposed by John Sidles, exploits magnetic resonance techniques to create spatial contrast [5]. As shown in Fig. 1, an MRFM sample is mounted in a uniform background magnetic field that partially polarizes the spins of the nuclei and unpaired electrons in the sample. Along with the background field, a near-by ferromagnet produces a position-dependent local magnetic field B_0 within the sample and exerts a force on the polarized spins. Either the sample or the ferromagnet is mounted on a microcantilever and the force between the two is observed by the deflection of the cantilever, which is monitored using a fiber optic interferometer [1].

Employing magnetic resonance techniques, sample spins can be made to flip periodically by a resonant radio frequency magnetic field oscillating at frequency f_{RF}. The resulting oscillating force causes an excitation of the cantilever. If the sample spins are flipped at the resonance frequency of the loaded cantilever f_C, the amplitude of the excitation is enhanced by a factor of the cantilever resonance quality factor Q relative to the low frequency response.

Due to the presence of the magnetic field gradient of the ferromagnet, only spins that are within a sensitive slice defined by the condition $f_{RF} = \gamma B_0/2\pi$ are flipped. The existence of a sensitive slice and the ability to scan the relative position of sample and ferromagnet give rise to a contrast mechanism that can be used to image spatially varying properties of the sample such as isotopic concentration [6] or spin-polarization [7]. State-of-the-art experiments have detected and resolved individual unpaired electrons in dilute samples [8]. Efforts are under way to push the sensitivity and resolution of MRFM technology to the single proton level, where three-dimensional imaging of single molecules may become feasible.

2.2 Army and Department of Defense Interest in MRFM

MRFM has the potential to be a key strategic technology. As a microscope, even at current sensitivities, it has potential to impact the development of electronic sensors and spintronic components in future Army systems. MRFM and related technologies may also be developed as biomolecular sensors in and of themselves. With atomic sensitivity and resolution, the future MRFM microscope will literally be radar for molecules, opening up broad unexplored frontiers of chemical space.

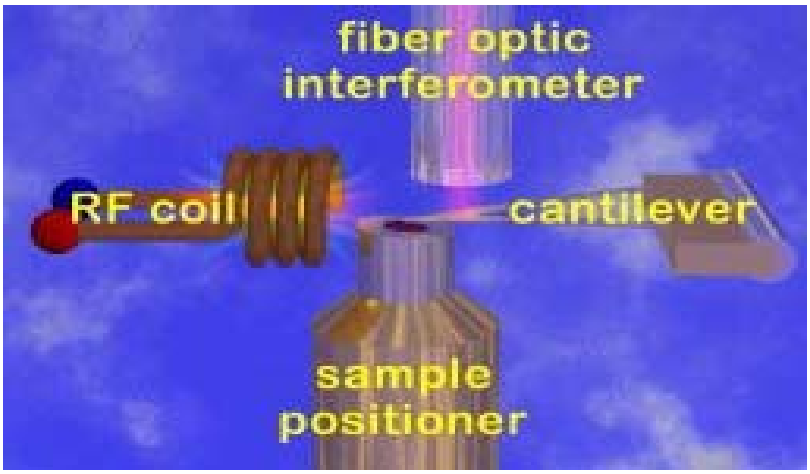

Figure 1. Diagram of a typical MRFM experiment. Changes in the sample that are induced by the RF field exert a periodic force on the cantilever. This force is observed by monitoring the motion of the cantilever with a fiber optic interferometer. Images are collected by monitoring the cantilever response as the sample is moved to various locations by the sample positioner.

The Army and the Department of Defense have a long history of supporting the development of MRFM technology. The Army Research Laboratory has maintained an active MRFM research program since 1996. Additionally, the Army Research Office has funded development of MRFM technology in universities and small businesses through multiple Small Business Technology Transfer grants. A three-year focused Defense Advance Research Projects Agency program played a critical role in the achievement of single-electron sensitivity. Most recently, the Army Research Office awarded substantial Multidisciplinary University Research Initiative grants to the University of Washington and Ohio State University with the goal of moving the technology to single-proton sensitivity within the next five years.

2.3 Quantum Limits to the Force-Sensitivity of a Mechanical Oscillator

Historically, MRFM sensitivity has maintained Moore's-law style progress, doubling every 3.1 months over the last decade [9]. If this trend continues, single-proton sensitivity will be achieved by 2010. This remarkable progress has been achieved by building instruments that are progressively smaller, colder and quieter according to design rules based on an analysis of the cantilever oscillators as classical objects at finite temperature. While clearly predicting which design changes will lead to improved sensitivity, this classical analysis predicts no ultimate limit to the sensitivity of any design as the temperature is reduced toward absolute zero (ref). Ultimately, quantum mechanics must limit the sensitivity of any instrument, even in the absence of thermal fluctuations. If single-proton sensitivity is to be achieved by following the classical design rules, researchers must be cognizant of the quantum limits to the accuracy of the classical analysis in order to avoid erroneous conclusions about the performance of their designs.

3 Body

3.1 Quantum Mechanical Analysis of Force Measurement Using a Mechanical Oscillator and Optical Interferometer

The objective in an MRFM experiment is to infer the force exerted on the cantilever by the sample by incorporating the cantilever into an interferometer and monitoring the behavior of light as it passes through it. In what follows, we systematically analyze the operation of the cantilever-interferometer system, applying quantum mechanics to determine what can and cannot be inferred about the external forces acting on the cantilever based solely on the interferometric data. In this analysis, we assume that the state of the individual photons entering the interferometer is uncorrelated with the state of the cantilever. This is consistent with the idea that the outcome of a well-designed measurement should depend only on the state of the system being measured and not on the initial state of the measuring device. Further, we assume that the photons have a definite wave number k, enter the interferometer at a uniform rate of ν photons per second that is much higher than the natural frequency of the mechanical oscillator under observation and are counted with unit efficiency by a detector at each exit channel of the interferometer. These assumptions will allow us to reach definite conclusions about force noise without detailed analysis of the much slower natural evolution of the cantilever. Because the response of the cantilever is linear, we can extrapolate these results to situations where the measurements are continuous and carried out over periods that are comparable to or longer than the period of the oscillator.

3.2 Ideal Optical Couplers

An ideal coupler, shown schematically in Fig. 2, is lossless and operates symmetrically, transmitting a percentage T of the light in each channel and reflecting a percentage R of the light in each channel into the other channel. Under these conditions, the probability amplitudes for all paths through the device are fixed up to an arbitrary common phase. In the case of a 50:50 coupler, half of the light that enters one channel exits in the other channel with probability amplitudes given by

$$\begin{aligned} |a\rangle &\rightarrow \frac{1}{\sqrt{2}}|a\rangle + \frac{i}{\sqrt{2}}|b\rangle, \\ |b\rangle &\rightarrow \frac{i}{\sqrt{2}}|a\rangle + \frac{1}{2}|b\rangle. \end{aligned} \tag{3.2.1}$$

For a 0:100 coupler (a mirror), the probability amplitudes for passage through the coupler are given by

$$\begin{aligned} |a\rangle &\rightarrow i\,|b\rangle, \\ |b\rangle &\rightarrow i\,|a\rangle. \end{aligned} \tag{3.2.2}$$

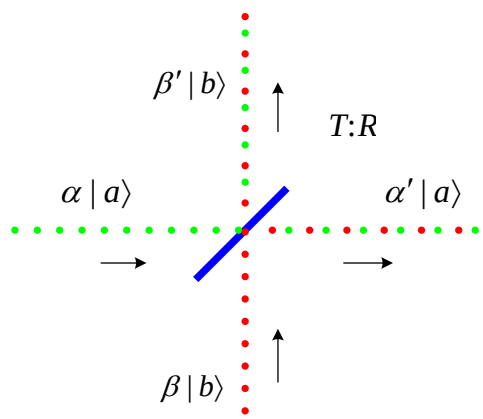

Figure 2. An ideal coupler transmits a percentage T of the light incident on it and reflects a percentage R of the incident light. This has the effect of mixing light that enters from the left with light that enters from the bottom of the diagram. The inherent symmetry between the a and b channels can be exploited to determine the effect of the coupler on the phase of the photons that pass through it up to an arbitrary common phase factor.

3.3 Ideal Optical Interferometer

An ideal interferometer, as shown in Fig. 3, is constructed from two 50:50 and two 0:100 couplers. Individual photons of wave number k enter channel a from an isolated source at a regular interval $1/\nu$, pass through the interferometer and are detected in either channel a or channel b by counters at the outputs. The probability amplitudes for each possible outcome are functions of the position χ of the 0:100 mirrors, which we take to be part of a quantum harmonic oscillator. Ultimately, we treat χ as a quantum observable related to the displacement x of an oscillator from equilibrium. Using the probability amplitudes for passage through the individual couplers presented in section 3.2, we find the final state of a photon that enters the interferometer through channel a:

$$|\,a\rangle \rightarrow \frac{\exp(i2k\chi)+1}{2}\,|\,a\rangle + \frac{\exp(i2k\chi)-1}{2i}\,|\,b\rangle\,. \tag{3.3.1}$$

3.4 Interferometer Tuning and Calibration

The interferometer must be properly tuned in order to observe very small changes in χ. Tuning is achieved when $\chi = x_0 + x$ is such that half of the photons go to each detector when $x = 0$. This occurs when $x_0 = \pi\,(n + 1/4)\,/\,k$ where n is any integer. Then the state of a photon that passes through the interferometer is given by

$$|\,a\rangle \rightarrow \frac{i\exp(i2kx)+1}{2}\,|\,a\rangle + \frac{i\exp(i2kx)-1}{2i}\,|\,b\rangle\,. \tag{3.4.1}$$

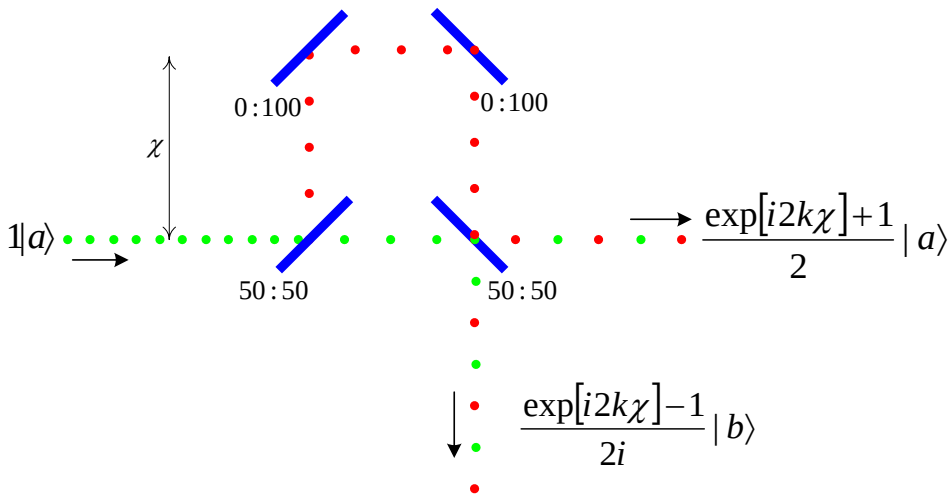

Figure 3. An ideal interferometer splits an incoming ray of light, allows the split beam to propagate along two distinct paths and then recombines the light to produce interference effects. The amplitude of the light that exits each channel of the interferometer depends on the difference in the lengths of the two paths. Observation of the rates at which photons arrive at each detector constitutes a measurement of the distance χ. The arrival of individual photons at each detector is a statistical process with the probabilities of the two possible outcomes governed by the laws of quantum mechanics. A large number of photons must be counted to obtain an accurate estimate of χ.

When the interferometer is tuned, the difference between the probability for a photon to be observed in channel *a* and the probability for a photon to be observed in channel *b* is related to *x* by

$$x = \frac{P_a - P_b}{2k}, \tag{3.4.2}$$

where we have assumed that *x* is much less than the wavelength of the interferometer light to neglect higher order terms.

The position of the oscillator is estimated by operating the interferometer for a period Δt and counting the number of photons N_a and N_b in each channel. Then

$$x_{\text{est}} = (N_a - N_b) / (2kN), \tag{3.4.3}$$

where $N = N_a + N_b = \nu \Delta t$.

3.5 Intrinsic Uncertainty in the Position Estimate

For a finite measurement period Δt, N_a/N and N_b/N are only approximations of the probabilities P_a and P_b. From elementary probability theory [10] and the observation that tuning implies $|N_a - N_b| << N$, the variance of x_{est} is

$$\sigma^2_{x\,\text{est}} = 1 / (4k^2 \nu \Delta t). \tag{3.5.1}$$

When the data record of photon counts in each channel is used to construct a continuous estimate of the position of the oscillator, there will be broad band fluctuations in the signal that arise solely from the discrete nature of the underlying measurement. Because the rate at which photons are counted is much higher than the frequency of the oscillator or any force we hope to observe, the noise appears to have a frequency-independent power spectrum S_x. For such white noise, the power spectrum is readily obtained from the variance in the position estimate:

$$S_x = 1 / (4k^2 \nu). \tag{3.5.2}$$

3.6 Interferometric Observation of a Quantum Object

To treat both the interferometer and the mechanical oscillator quantum mechanically, we must determine how the combined quantum state of the system evolves between introduction of the photon and its subsequent detection. Under the assumptions of section 3.1, the photon-oscillator system is initially prepared in an uncorrelated product state

$$|\psi_{\text{initial}}\rangle = \psi_0(x) \otimes |a\rangle, \tag{3.6.1}$$

where $\psi_0(x)$ is the wavefunction of the oscillator just prior to the measurement.

After the photon passes through the interferometer, but before it is detected in either channel a or b, the photon and oscillator are in an entangled state

$$|\psi_{\text{initial}}\rangle = A(x)\psi_0(x) \otimes |a\rangle + B(x)\psi_0(x) \otimes |b\rangle, \tag{3.6.2}$$

where

$$A(x) = \frac{i\exp(i2kx)+1}{2}, B(x) = \frac{i\exp(i2kx)-1}{2i}. \tag{3.6.3}$$

Subsequently, exactly one photon is observed in either channel a or channel b. The photon is destroyed and the oscillator is left in the state

$$\psi(x) = \frac{A(x)\psi_0(x)}{\sqrt{P_A}} \text{ or}$$
$$\psi(x) = \frac{B(x)\psi_0(x)}{\sqrt{P_B}}, \tag{3.6.4}$$

with probability

$$P_A = \int_{-\infty}^{+\infty} \psi^*(x) A^*(x) A(x) \psi_0(x)\, \mathrm{d}x \text{ or}$$
$$P_B = \int_{-\infty}^{+\infty} \psi^*(x) B^*(x) B(x) \psi_0(x)\, \mathrm{d}x \tag{3.6.5}$$

Respectively [11].

This sequence of events is repeated for each photon and the effects on the state of the oscillator are cumulative. After a large number of iterations, the probability density becomes sharply peaked at x_{est}. It can be shown through analysis of the density matrix that were the measurement performed on an ensemble of identically prepared oscillators, the resulting set of values of x_{est} would conform to the original quantum probability distribution for the position of the oscillator

$$P(x)dx = |\psi_0(x)|^2 \mathrm{d}x. \tag{3.6.6}$$

This self consistency is necessary for a legitimate measurement of the position as a quantum observable.

3.7 Quantum Back Action on the Oscillator

In quantum mechanics the variance of the linear momentum of an object necessarily increases when the variance of the position decreases, as happens during the measurement of the position of the oscillator described in section 3.6. This behavior of the oscillator is equivalent to its response to the application of an external white-noise force. The effect is called back action, and it cannot be distinguished from an external force acting on the cantilever by examining the data record. Back action contributes to the signal when a cantilever and interferometer are used to measure an external force. Ultimately, this limits the force sensitivity of the system.

The power spectral density of the back-action force is related to the rate of change of the variance of the linear momentum by

$$S_{F\mathrm{ba}} = \mathrm{d}\,\sigma^2_p / \mathrm{d}\,t. \tag{3.7.1}$$

The Heisenberg uncertainty principle,

$$\sigma_x^2 \sigma_p^2 \geq \frac{\hbar^2}{4}, \tag{3.7.2}$$

along with the uncertainty in the position of the oscillator after the measurement, sets an absolute lower limit on the back-action force of

$$S_{F\,\mathrm{ba}} \geq \hbar^2 k^2 \nu. \tag{3.7.3}$$

Because we have developed a microscopic model of the photon-oscillator interaction, it is possible to calculate the rate of change of the variance of the linear momentum analytically. To do this, we start by assuming that the oscillator is initially in the state

$$\psi_0(x) = \left(\frac{a}{2\pi}\right)^{1/4} \exp\left(-ax^2\right), \tag{3.7.4}$$

where a is a constant that is proportional to the initial variance of the oscillator position. Ultimately, the calculation only relies on the fact that the initial linear momentum of the oscillator is zero and the initial probability density of the oscillator position is concentrated near $x = 0$. Further, if the interferometer acts as a robust measuring device, it is reasonable to assume that the power spectral density of the back-action force is insensitive to the initial state of the oscillator and its eventual evolution under the influence of its own Hamiltonian. We also assume that the spectral density of the back action is insensitive to the actual data record. As a matter of combinatorics, the largest and most probable group of possible data records has $N_a = N_b = n$ after $2n$ iterations. The net effect of the quantum back action depends on N_a and N_b, but does not depend on the order in which the photons arrive in the counters, so we can do a single calculation for this large group of data records and take it to be representative of the general behavior.

The expectation value of linear momentum, initially zero, becomes

$$\langle p_{2n} \rangle = (\hbar k) 2n \tag{3.7.5}$$

due to the mean photon pressure exerted by the reflected photons. Using this fact and the assumptions detailed above, the rate of change of the variance of the linear momentum is given by

$$\frac{\mathrm{d}}{\mathrm{d}\,t}\sigma_p^2 \cong \frac{\langle \left(p_{2n} - \langle p_{2n} \rangle\right)^2 \rangle - \langle \left(p_{2(n-1)} - \langle p_{2(n-1)} \rangle\right)^2 \rangle}{2n/\nu - 2(n-1)/\nu} \cong 2\hbar^2 k^2 \nu, \tag{3.7.6}$$

and the corresponding back action force power spectral density is

$$S_{F\,\mathrm{ba}} = 2\hbar^2 k^2 \nu, \tag{3.7.7}$$

a factor of two larger than the minimum value consistent with the uncertainty principle. It is important to note that either increasing the wave number of the interferometer light or increasing the rate at which photons are sent through the interferometer in an effort to reduce the noise in the position data has the possibly undesirable effect of increasing the back action force.

3.8 Implications of Quantum Back Action on the Measurement of Forces

When a force is measured by monitoring the position of a mechanical oscillator such as a microcantilever, a balance must be struck between positional accuracy and back action force to achieve optimal results. When the frequency of the force to be measured is much lower than the natural frequency of the oscillator, the oscillator response is $x(t) = k_s/F(t)$, so the net power spectral density of the noise in the measured force, which has contributions from the noise in the measured position and the back action force from the interaction with interferometer photons, is

$$\begin{aligned} S_{F\,\text{measured}} &= k_s^2 S_x + S_{F\,\text{ba}} \\ &= k_s^2 \frac{1}{4k^2\nu} + 2\hbar^2 k^2 \nu. \end{aligned} \tag{3.8.1}$$

The net noise in the measured force is minimized when the two contributions are equal. This occurs when the optical power through the interferometer, written here in terms of the photon wavelength λ, is

$$P = \frac{c k_s \lambda}{2\pi\sqrt{8}}. \tag{3.8.2}$$

At this optimal optical power, the net power spectral density of the noise in the measured force is

$$S_{F\,\text{measured}} = \sqrt{2} k_s \hbar \tag{3.8.3}$$

In a state-of-the-art MRFM experiment, $k_s = 10^{-6}$ N/m and $\lambda = 10^{-6}$ m are typical values for the spring constant and operating interferometer wavelength. This gives a quantum limited force noise and optimal optical power of $\sqrt{S_{F\text{measured}}} = 0.01$ aN Hz$^{-1/2}$ and $P = 20$ μW respectively. By way of comparison, typical estimates of the force in a single-proton MRFM experiment are in the range of 1 to 0.1 aN [12].

4 Conclusion

The result of the calculation presented in Section 3 is encouraging. It says that quantum mechanics does not preclude observation of individual protons by state-of-the-art MRFM instruments with laboratory time scale signal averaging. If the classical analysis predicts adequate sensitivity, we can expect the experiment to achieve the anticipated results. There is no reason to abandon the design rules that led to single-electron sensitivity in the quest for single-

proton sensitivity. By building progressively smaller, colder, quieter instruments it should be possible to achieve the necessary force sensitivity.

Finally, we note that environmental effects including thermal fluctuations can be modeled as a suitable set of measurement processes and feedback controls. Modeling environmental effects in this manner provides a tangible link between the decoherence of the quantum state and the accumulation of information about the state of the system by the environment and eliminates the need to introduce ad hoc relaxation processes to finite-temperature simulations. We have found that a distinct advantage of this method of incorporating environmental effects into simulations of quantum systems is that it selectively suppress any long-range quantum correlations that are particularly susceptible to decoherence by the environment. The quantum behavior of systems modeled this way can be accurately and efficiently simulated, even for systems with long-range interactions and no spatial order, provided the system has sufficient coupling to the environment to prevent it from acting as a quantum computer. The efficiency gains appear to be due to a dynamic confinement of the trajectory of the state of the quantum system to a small region of the total state space without adversely affecting the accurate prediction of experimental results.

This work is supported in part by the Army Research Office, the Defense Advanced Research Projects Agency, the National Science Foundation and the National Institutes of Health.

References

1. D. Rugar, H. J. Mamin, and P. Guethner, *Appl. Phys. Lett.* **55**, 2588 (1989).

2. H. J. Mamin and D. Rugar, *Appl. Phys. Lett.* **79**, 3358 (2001).

3. J. A. Sidles, J. L. Garbini, K. J. Bruland, D. Rugar, O. Züger, S. Hoen and C. S. Yanoni, *Rev. Mod. Phys.* **67**, 249 (1995).

4. David D. Awschalom, Robert Buhrman, James M. Daughton, Stephan von Molnar and Michael L. Roukes, *Spin Electronics*, (Dordrecht : Springer, 1999).

5. J. A. Sidles, *Appl. Phys. Lett.* **58**, 2854 (1991).

6. O. Züger, S. T. Hoen, C. S. Yannoni and D. Rugar, J. Appl. Phys. 79, 1881 (1996).

7. Kent R. Thurber, Lee E. Harrell, Raúl Fainchtein and Doran D. Smith, *Appl. Phys. Lett.* **80**, 1794 (2002).

8. D. Rugar, R Budakian, H. J. Mamin and B. W. Chui, *Nature* **430**, 339 (2004).

9. J. A. Sidles and Joseph L. Garbini, "Imaging of Molecules by Oscillator-Coupled Resonance," available at www.mrfm.org.

10. Charles Kittel and Herbert Kroemer, *Thermal Physics*, 2nd Ed., 10-23 (San Francisco: W. H. Freeman and Company, 1980).

11. Michael A. Nielsen and Isaac L. Chuang, *Quantum Computation and Quantum Information*, (Cambridge: Cambridge University Press, 2000).

12 Joseph L. Garbini and John A. Sidles, "Program for Achieving Single Nuclear Spin Detection: A UW Quantum System Engineering White Paper," 26 February 2005, available at www.mrfm.org.